ACS APPLIED MATERIALS & INTERFACES

Research Article

www.acsami.org

Three-Dimensional Cu_2ZnSnS_4 Films with Modified Surface for Thin-Film Lithium-Ion Batteries

Jie Lin, Jianlai Guo, Chang Liu, and Hang Guo*

Pen-Tung Sah Micro-Nano Science and Technology Institute, Xiamen University, Xiamen, Fujian 361005, China

Supporting Information

ABSTRACT: Cu_2ZnSnS_4 (CZTS) is an important material in low-cost thin film solar cells and is also a promising candidate for lithium storage. In this work, a novel three-dimensional CZTS film coated with a lithium phosphorus oxynitride (LiPON) film is fabricated for the first time and is applied to thin-film lithium-ion batteries. The modified film exhibits an excellent performance of ~900 mAh g^{-1} (450 μAh cm^{-2} μm^{-1}), even after 75 cycles. Morphology integrity is still maintained after repeated lithiation/delithiation, and the main reaction mechanism is analyzed in detail. The significant findings from this study indicate the striking advantages of modifying both the surface and structure of alloy-based electrodes for energy storage.

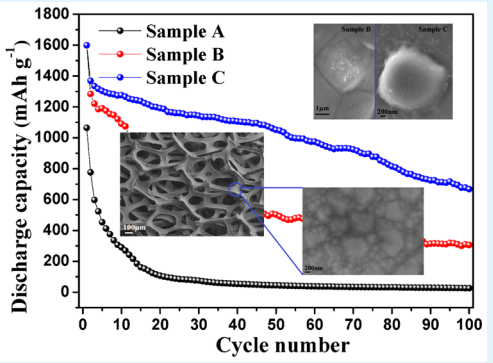

KEYWORDS: *Cu_2ZnSnS_4, lithium phosphorus oxynitride, Ni foam, thin film, lithium-ion battery*

1. INTRODUCTION

The development of micropower sources is an emerging requirement for meeting the need to supply energy to micro/nano devices and micro electromechanical system (MEMS).[1] Thin-film lithium-ion batteries (LIBs)[2,3] have been receiving worldwide attention, because of their flexible size, safety, high energy density, and the possibility of on-chip integration. However, because conversion or alloying reactions[4] can offer a high theoretical capacity, the capacity of the commonly used graphite[5] is considered to be too low for the application in advanced thin-film LIBs. Binary metallic sulfides (such as CuS, ZnS, SnS, FeS, etc.) with high capacities have been examined as promising anode materials in the next-generation LIBs.[6−9] However, the wide application of these materials is hindered by their severe capacity degradation after the first several cycles. Currently, tremendous efforts have been devoted to combining the unique properties of individual constituent elements and components to address this problem, e.g., the combination of Cu−Sn−S film,[10] the introduction of carbon-coating into SnS,[11] and the integration of Sn−Zn−Cu multilayer film,[12] all of which improve the conductivity and capacity of the sulfides. Therefore, the use of the various elements in the Cu_2ZnSnS_4 (CZTS) quaternary compound is highly advantageous for lithium storage; in addition, the CZTS film fabricated by magnetron sputtering is uniform with a well-defined composition.

Because of their direct band gap of 1.5 eV and a large absorption coefficient (>10^4 cm^{-1}),[13] CZTS films are well-known to be the absorption layer in low-cost thin-film solar cells. Sn and Zn elements in the CZTS are electrochemically active toward Li,[14] so multiple lithiation reactions can be expected in this substantial material. In addition, CZTS films offer the possibility of using such a multifunctional material for bridging solar cells and LIBs. Because the electrochemical reactions may be complex, the investigation of CZTS film for lithium storage is of great significance and interest. On the other hand, a widely used solid-state electrolyte, lithium phosphorus oxynitride (LiPON),[15−17] which is generally obtained by sputtering Li_3PO_4 in a N_2 atmosphere, can transport Li^+ and has a wide electrochemical window (>5.5 V). Because the disordered nature of LiPON can modify the surface potential and facilitate Li^+ adsorption,[18] LiPON has been used as a protective film for $LiCoO_2$, $LiMn_2O_4$, $LiNi_{0.5}Mn_{1.5}O_4$, silicon, and other materials.[19−22] Nevertheless, LiPON has not been used as an alleviating buffer for alloys including CZTS. Optimization of the interface between electrodes and electrolyte is often an effective approach to improve the poor cycle performance, and LiPON film is highly favored to serve as the protective layer. Thus, coupling these two potential materials may enable the combination of a high capacity and good cycle performance.

Consequently, we here report for the first time a three-dimensional (3D) CZTS film deposited by magnetron sputtering as an anode material for thin-film LIBs. Moreover, the surface is modified by the LiPON film to form a pomegranate-shaped structure. Benefiting from the advantages of a fast ionic conductor and 3D substrate, the modified sample delivers a remarkable electrochemical performance of ~900

Received: May 21, 2015
Accepted: July 20, 2015
Published: July 20, 2015

DOI: 10.1021/acsami.5b04421
ACS Appl. Mater. Interfaces 2015, 7, 17311−17317

mAh g^{-1} (450 μAh cm^{-2} μm^{-1}) even after 75 cycles, that is superior to the reported CZTS materials[23−26] (680 mAh g^{-1} after 40 cycles for the best case) and other thin-film LIB anodes[27] (206 μAh cm^{-2} μm^{-1} for Li metal). The novel 3D multilayer thin films provide insight into a promising direction for the future development of high-performance anode materials.

2. EXPERIMENTAL SECTION

2.1. Fabrication of Films. All films were fabricated using radio frequency (RF) magnetron sputtering (Model JC500-3/D magnetron sputtering system, China). Planar nickel foils (0.05 mm thick) and nickel foams (0.5 mm thick) were used as the substrates. The fabrication process is schematically illustrated in Figure 1. After

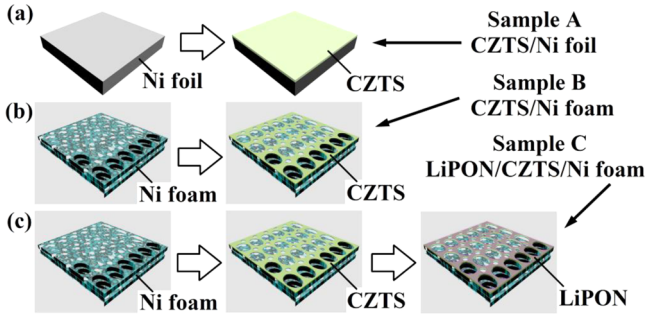

Figure 1. Fabrication process and structures of (a) sample A, (b) sample B, and (c) sample C.

cleaned by sonication in acetone, ethanol, and deionized (DI) water in sequence for 10 min each, a CZTS film (~1 μm) was deposited on the nickel foils and nickel foams by sputtering a 4-in CZTS target (purity, 99.99%). The chamber pressure was kept at 1.3 Pa in an argon atmosphere, and the sputtering power was 120 W. The planar CZTS film on nickel foils and the 3D CZTS film on nickel foams are denoted as samples A and B, respectively. A LiPON film (~100 nm) was then deposited on sample B by sputtering a 4-in Li_3PO_4 target (purity, 99.99%) in a N_2 atmosphere. The chamber pressure was kept at 1.3 Pa, and the sputtering power was 100 W. The obtained 3D LiPON/CZTS/Ni foam film is denoted as sample C.

2.2. Material Characterizations. Small pieces with a size of 10 mm × 10 mm were cut from the prepared samples. The effective mass of CZTS film on each substrate is ~0.5 mg. X-ray diffraction (XRD) (Rigaku Ultima IV) was used to identify the microstructure. The morphology and elementary composition were investigated using ZEISS Sigma scanning electron microscopy (SEM) and high-resolution transmission electron microscopy (HRTEM FEI Tecnai-F30) systems, both equipped with an energy-dispersive X-ray (EDX) analyzer. The TEM samples were prepared by depositing a drop of diluted suspension in ethanol on a copper grid coated with a carbon film.

2.3. Electrochemical Measurements. The electrochemical properties of the films were measured in coin cells (CR2016) assembled in an argon-filled glovebox. The prepared samples were chosen as the working electrodes, lithium metal foils as the counter electrodes, a polypropylene film (Celgard 2400) as the separator, and 1.0 M $LiPF_6$ mixed with ethylene carbonate, dimethyl carbonate and diethyl carbonate (EC/DMC/DEC, 1:1:1 in volume) as the electrolyte. After the cells were shelved for ~12 h, galvanostatic charge/discharge tests were conducted using Model Neware BTS-5 V/1 mA battery test systems (Shenzhen, China) with a voltage range of 0.01−3 V and a current density of 100 mA g^{-1}. Cyclic voltammetry (CV) tests were performed using Model Arbin-BT2000 battery test instruments between 0 and 3.0 V at a scanning rate of 0.5 mV s^{-1}. Electrochemical impedance spectroscopy (EIS) was tested using a Model CHI660E electrochemical workstation (CH Instruments), with an amplitude potential of 5 mV and a frequency range from 0.1 Hz to 1 MHz. All tests were conducted at room temperature.

3. RESULTS AND DISCUSSION

3.1. Morphology and Structural Properties. The surface image of sample A is depicted in Figure 2a1. Large quantities of evenly distributed CZTS agglomerations can be seen clearly. The diameter of these spheres ranges from 100 nm to 900 nm. The magnified picture (Figure 2a2) shows that the CZTS sphere is constructed by amounts of different CZTS nanoparticles. This reveals that the severe capacity decay may be caused by the decomposition of clusters or agglomeration after repeated Li^+ insertion/extraction.[23] In addition, the compact coverage in planar substrate may aggravate the failure of active materials.

Figure 2a3 displays the 3D structure of nickel foams on a large scale. The loose structure with abundant open space for alleviating volumetric change can be expected to enhance the cycle performance of CZTS film for LIBs. In contrast to sample A and nickel foam, the entire surface of sample B (Figure 2b1−b3) is fully coated with CZTS particles of different diameters. The slit of CZTS spheres along the junction of nickel foam (Figure 2b3) indicates that the film tends to form a 3D structure with split particles during nucleation.

Examination of the morphology of sample C (Figure 2c1−c3) reveals that the coated film is composed of CZTS nanoparticles and the LiPON film. Several spheres are connected with each other to form large crystalline aggregations. Moreover, the surface of CZTS is uniformly covered by LiPON with a transparent feature. Herein, since the nickel foam serves as the backbone and LiPON acts as a protective film, the collapse of large spheres may be effectively restrained, preventing the severe capacity decay. The EDX pattern of sample C (Figure 2d) confirms the existence of copper, zinc, tin, sulfur, oxygen, phosphorus, and nitrogen, indicating the successful deposition of CZTS and LiPON on the Ni foams.

The cross-section images of all films are investigated by depositing CZTS and LiPON/CZTS films on silicon. As shown in Figures 2e and 2f, the interfaces between the layers are all smooth, without any pinholes or cracks. The uniform thickness of CZTS and LiPON is measured to be ~1 μm and ~100 nm, respectively. Because the LiPON film is too thin to be visible in the side view, the surface of CZTS film is evenly coated with a thin transparent film that is not as clearly seen as in Figure 2. The thin film acts as a physical buffer for preventing the direct contact between the CZTS film and electrolyte and is expected to release the volumetric change effectively.

The CZTS film morphology was also examined by TEM. The well-dispersed CZTS nanosheets (Figures 3a, 3b, and 3d) indicate that the CZTS film is assembled from nanoscale aggregations. The elementary composition of CZTS detected by EDX is shown in Figure 3c. The presence and atomic ratio of copper, zinc, tin, and sulfur evidence the successful deposition of CZTS film. The HRTEM image taken from the nanosheets is shown in Figure 3d. Three accordant lattice fringes with an interplanar spacing of 0.31 nm are resolved as the (112) crystal planes of tetragonal CZTS (JCPDS No. 26-0575), which is consistent with the (112) diffraction ring of the selected area electron diffraction (SAED) pattern (Figure 3e). To eliminate the distraction of the nickel substrate, the CZTS film deposited on the silicon substrate and the powders of CZTS target are both studied by XRD (Figure 3f). Differing

DOI: 10.1021/acsami.5b04421
ACS Appl. Mater. Interfaces 2015, 7, 17311−17317

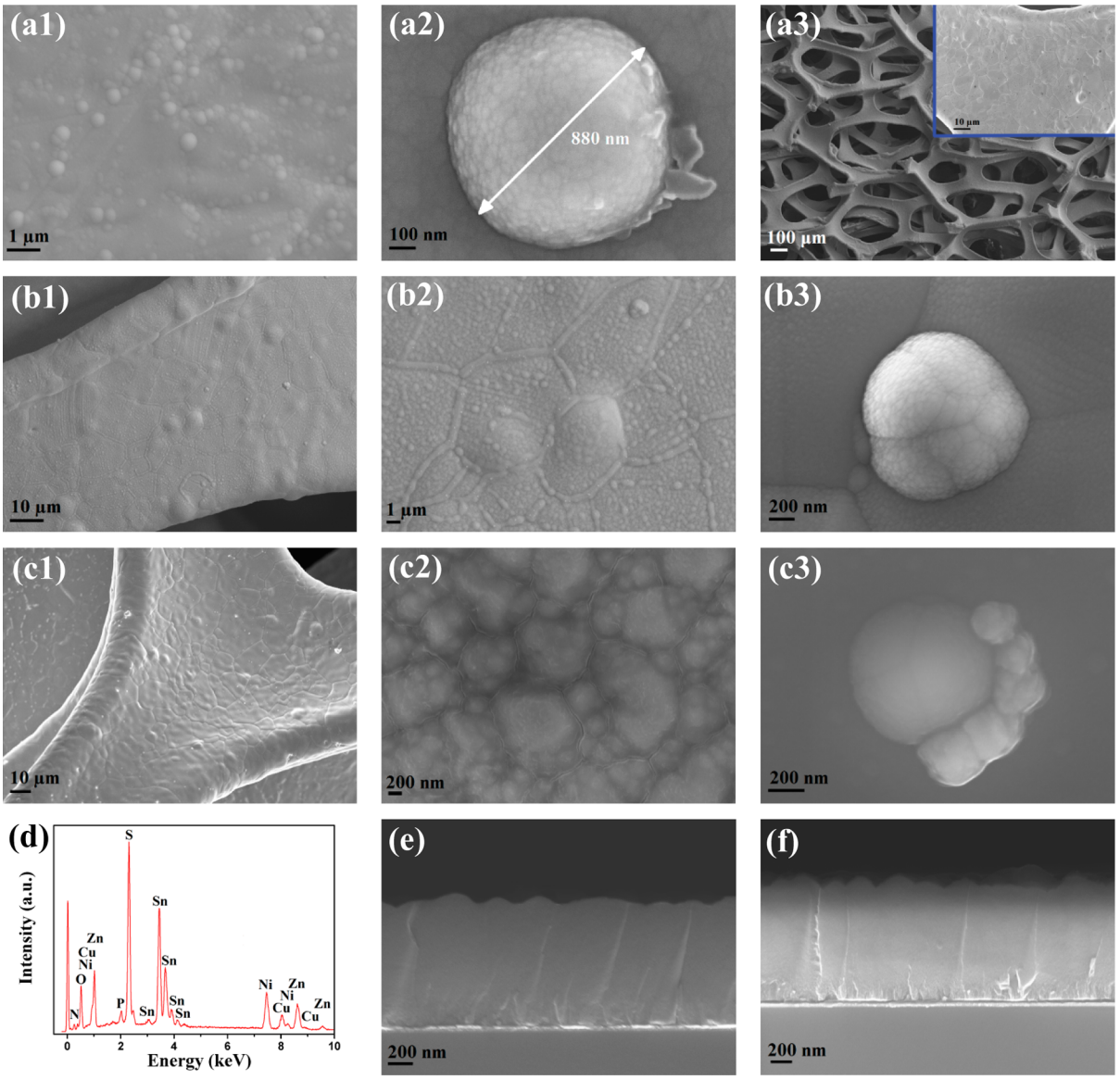

Figure 2. Surface SEM images of (a1, a2) sample A, (a3) Ni foam, (b1−b3) sample B, and (c1−c3) sample C. (d) EDX spectra of sample C. (e, f) Cross-section SEM images of samples B and C on silicon.

from the target, the single diffraction peak of CZTS film at 2θ = 28.5° is related to the (112) plane of tetragonal CZTS with the sulfur in a face-centered cubic sublattice,[28] in agreement with the TEM results. All these results demonstrate the high quality of the CZTS film successfully fabricated via magnetron sputtering.

3.2. CV and EIS Tests. The reaction mechanism of all samples is characterized by CV tests and compared with the CV curves of ZnS and SnO_2 films (see Figures S1 and S2 in the Supporting Information). Because the CV curves of all samples are quite similar, sample C is chosen as the representation for the purposes of discussion (Figure 4a). In the initial scan, several oxidation peaks at 0.75, 1.2, 1.5, 1.9, and 2.4 V are observed, and reduction peaks at 0.01, 0.3, and 0.8 V are displayed. The oxidation peaks do not obviously change with the increased cycle number. However, the initial reduction peak at 0.8 V arising from eq 1 first disappears,[23] and then divides into two peaks of 1.1 and 0.9 V, corresponding to eqs 2 and 3, respectively.[7,8] In particular, the anode peaks at 0.75, 1.5, and 1.9 V can be due to the Sn reactions specified by eq 2.[8,25] The anode peaks due to the Zn reactions appear at 1.2, 1.9, and 2.4 V.[7,25] The cathode peaks at ∼0.01 V and ∼0.3 V are due to the reactions described by eqs 2 and 3, collectively.[26] Consequently, the electrochemical reactions are mainly assigned to the alloying of Li−Sn and Li−Zn. As marked in the CV curves of sample A (Figure 4b), the anode peaks at ∼1.7 V and the cathode peaks at ∼1 V related to eq 1 are greatly reduced with cycling. Considering the multistep reactions of eqs 1−3 with the accumulated Li_2S and soluble sulfides in the electrolyte, it is reasonable to believe that the reduced reversible reaction will cause an inevitable capacity decay, as well as the inherent weakness of alloy-based sulfides. In addition, the formation of solid electrolyte interphase (SEI) film mainly occurs between 0.4 V and 1.2 V in the initial cycle (Figure 4c). The corresponding cathode peaks are more reduced in sample C than in sample B, indicating that the artificial film (LiPON) retards growth of the SEI layer.

$$Cu_2ZnSnS_4 + 8Li^+ + 8e^- \rightarrow 2Cu + Zn + Sn + 4Li_2S \quad (1)$$

DOI: 10.1021/acsami.5b04421
ACS Appl. Mater. Interfaces 2015, 7, 17311−17317

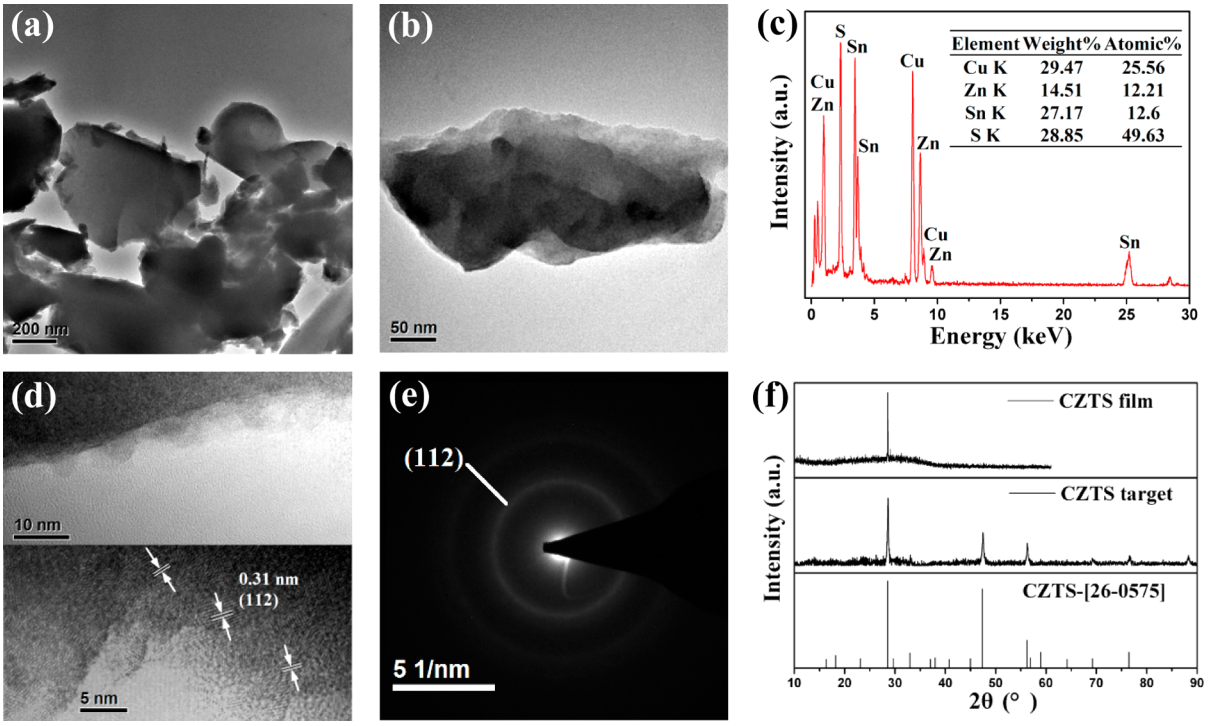

Figure 3. (a, b) TEM images, (c) corresponding EDX spectra, (d) HRTEM images, and (e) SAED pattern of pristine CZTS film. (f) XRD patterns of CZTS target and CZTS film on silicon.

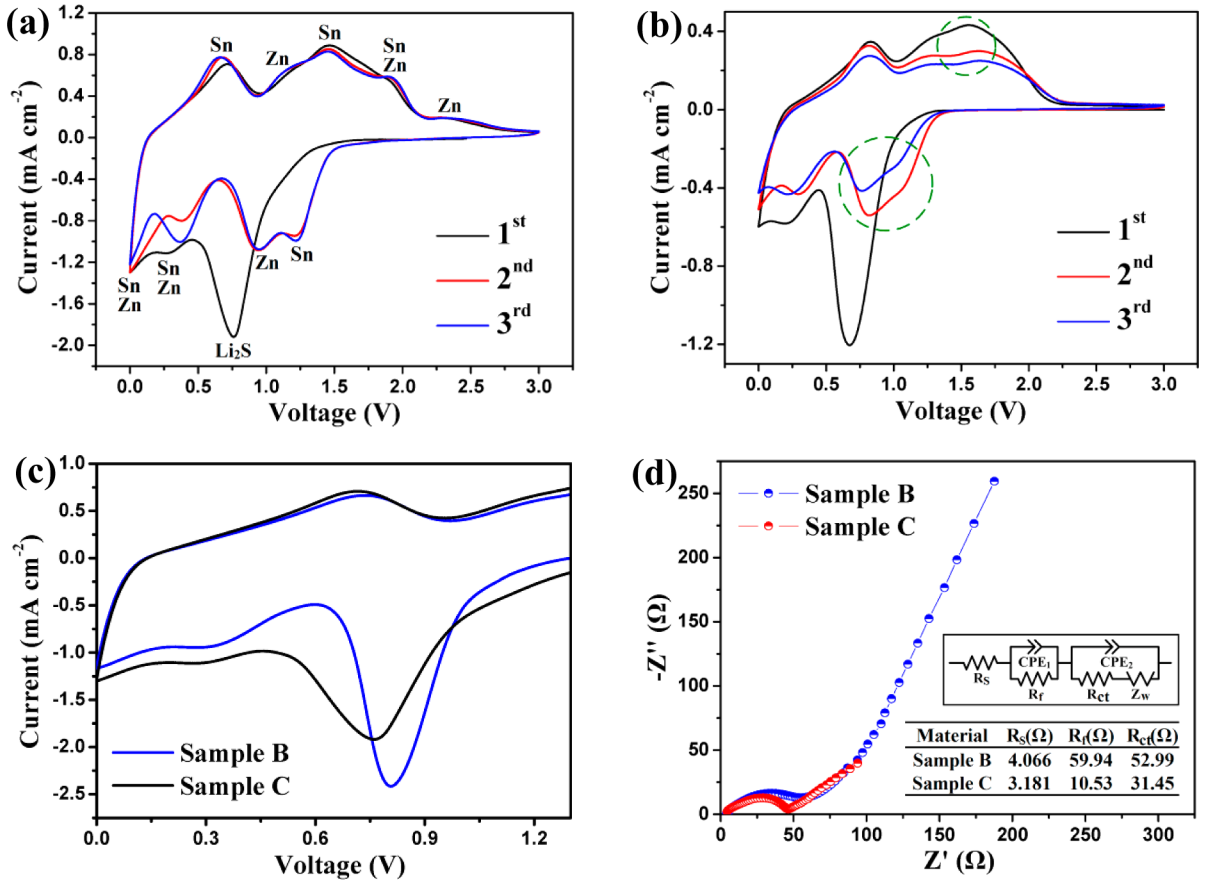

Figure 4. (a, b) CV curves of first three cycles of samples C and A. (c) Detailed view of CV curves of samples B and C between 0 and 1.25 V. (d) Initial EIS of samples B and C. Inset shows the equivalent circuit model and fitted impedance parameters.

DOI: 10.1021/acsami.5b04421
ACS Appl. Mater. Interfaces 2015, 7, 17311−17317

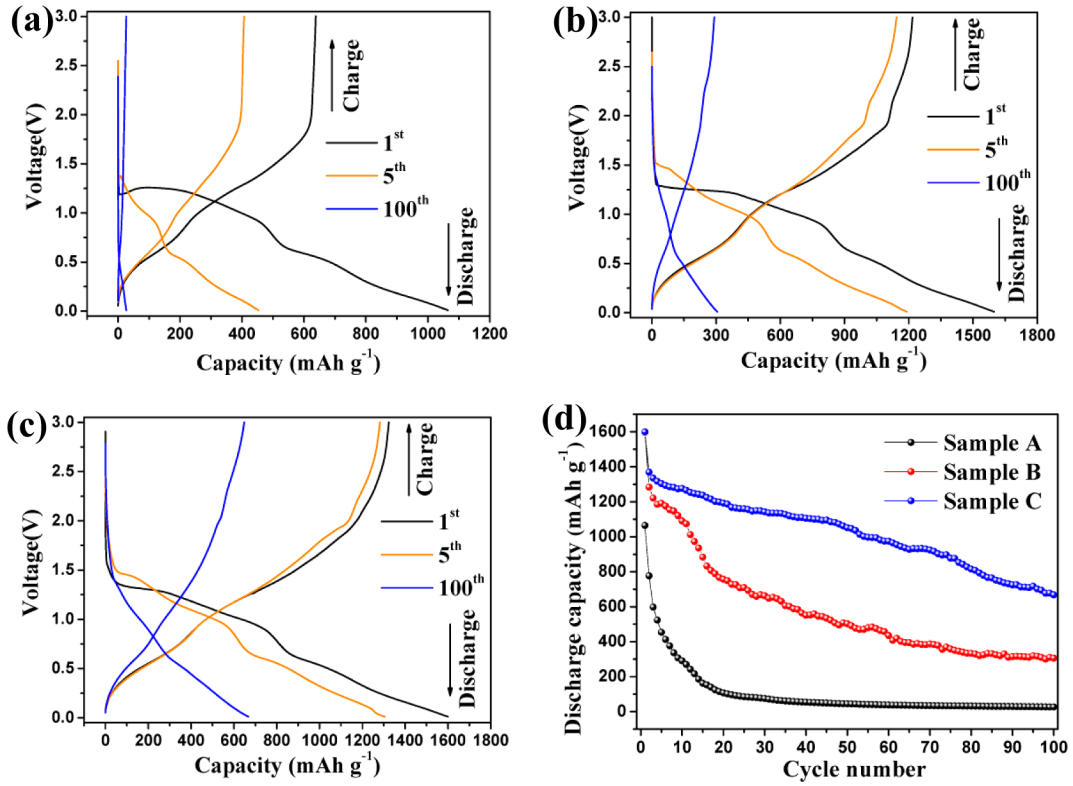

Figure 5. Galvanostatic charge/discharge curves of (a) sample A, (b) sample B, and (c) sample C. (d) Cycle performance of all samples at a current density of 100 mA g^{-1}.

$$\mathrm{Sn} + x\mathrm{Li}^+ + x\mathrm{e}^- \leftrightarrow \mathrm{Li}_x\mathrm{Sn} \qquad (0 \le x \le 4.4) \tag{2}$$

$$\mathrm{Zn} + x\mathrm{Li}^+ + x\mathrm{e}^- \leftrightarrow \mathrm{Li}_x\mathrm{Zn} \qquad (0 \le x \le 1.5) \tag{3}$$

The initial electrochemical impedance of samples B and C are measured by EIS tests (Figure 4d), with the equivalent circuit model shown in the inset of Figure 4d. In this circuit, R_s is the internal resistance of battery, R_f is the contact resistance of the SEI film, R_{ct} is the charge-transfer resistance of electrode/electrolyte interface, and W_{dif} is the Warburg impedance of Li^+ diffusion, respectively.[29] The fitted parameters are given in the inset table of Figure 4d. Conspicuously, because of the modified surface and the elevated Li^+ diffusion kinetics by LiPON film, the interface resistances of sample C are smaller than sample B, and the interface resistances of sample B are so large that result in an inferior cycle life. Moreover, the additional film prevents the direct contact between electrode and liquid electrolyte leading to smaller transfer resistances. As a result, the reduced resistances of sample C can greatly enhance the electrochemical performance.

3.3. Galvanostatic Charge/Discharge Tests. The galvanostatic charge/discharge curves of sample A are shown in Figure 5a. The current−potential characteristics are consistent with those reported for the CZTS materials and the above CV tests.[23,24,26] The initial charge and discharge capacities are 638 and 1065 mAh g^{-1} with an irreversible capacity loss of 40.1%. A broad discharge plateau at 0.8−1.25 V is observed, which then disappears in the following cycles. This plateau is generally ascribed to the formation of Li_2S, copper, zinc, tin, and SEI film as noted previously. Another discharge plateau at ∼0.4 V is associated with the Li−Sn and Li−Zn alloying. During the charge process, two steep plateaus at ∼0.5 and 1.25 V may be attributed to the Li−Sn and Li−Zn dealloying. In the fifth cycle, the Coulombic efficiency is ∼100% implying the cessation of side reactions. The curves also remain identical to that of the first cycle except for the reduced capacity and the irreversible broad plateau mentioned above. Because of the fact that the repeated Li^+ insertion/extraction in the large CZTS clusters may result in severe collapse or rupture, the capacity decays drastically after 100 cycles. The discharge capacity decreases to only 2.5% of the value obtained in the first cycle (26.6 mAh g^{-1} vs 1065 mAh g^{-1}).

Figure 5b presents the charge/discharge voltage profiles of sample B. The charge and discharge capacities in the first cycle are 1217 mAh g^{-1} and 1598 mAh g^{-1}, with an irreversible capacity loss of 23.8%, which is much less than that of sample A. The voltage plateaus in the first and fifth cycle are almost the same as those of sample A, suggesting the identical active material (CZTS film). In the 100th cycle, the discharge capacity of 306 mAh g^{-1} (more than 10 times greater than that of sample A) demonstrates the improved cycle performance. Moreover, the curves gradually become slopes, indicating the lithiation process-driven transition from crystal to amorphous phase[25] and the increased dissolution of sulfide.

The charge/discharge curves of sample C are presented in Figure 5c. The first charge/discharge capacities are 1323 mAh g^{-1} and 1600 mAh g^{-1} with an irreversible capacity loss of 17.3%. No obvious intergroup difference can be seen between the first and fifth cycle, showing the improved reversibility. As expected, the reversible capacity is the highest among all samples. Meanwhile, the voltage plateaus are the same as those observed in samples A and B, verifying that the additional LiPON does not suppress the lithiation reactions[30] but rather facilitates an excellent cycle performance.

The cycle performance of all samples is shown in Figure 5d. Typically, sulfides exhibit a striking drop after the first several

DOI: 10.1021/acsami.5b04421
ACS Appl. Mater. Interfaces 2015, 7, 17311−17317

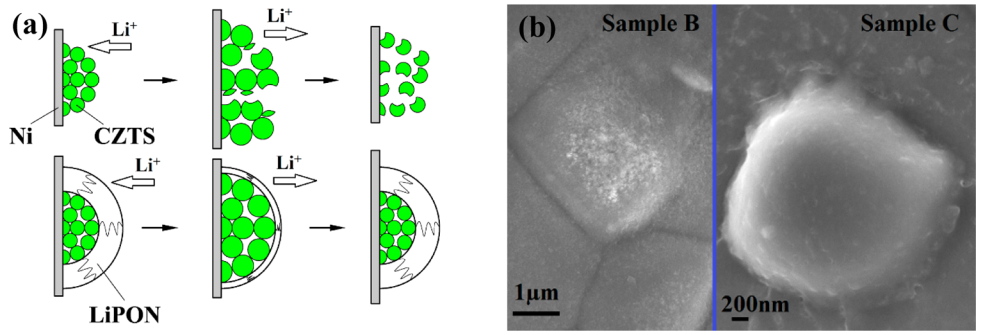

Figure 6. (a) Scheme of constrained electrochemical reaction process inside CZTS particles. (b) Post-mortem morphology of samples B and C after 100 cycles.

cycles[29] similar to the result for sample A. After 20 cycles, the capacity of sample A quickly falls to 107 mAh g^{-1}. The huge volumetric change and dissolution of active materials in alloy-based sulfides[31] is believed to be the origin of this effect. With the introduction of the 3D substrate, sample B exhibits an increased capacity (>900 mAh g^{-1}) in the first 15 cycles, signifying the released volumetric expansion. The capacity then begins to decay drastically, and this phenomenon may be caused by the accumulated byproducts and the destruction of active materials and microstructure. In contrast, because of the combination of high-performance materials, 3D structure, and modified surface, the capacity of sample C remains higher than 900 mAh g^{-1} in the first 75 cycles. After 100 cycles, the capacity value is still as high as 668 mAh g^{-1}. Both the prominent cycle performance and high capacity are superior to the reported results. We interpret this to be due to the prevention of structural collapse of aggregations by the pomegranate-shaped structure, the increased Li^+ diffusion kinetics inside CZTS by the additional Li^+ of LiPON and the porous 3D structure by the Ni foam substrate.

3.4 Post Morphologies. As shown in Figure 6a, the volumetric expansion of CZTS particles after repeated lithiation will lead to the crack or fracture of CZTS spheres, rendering the dissolution of active materials[32] and severe capacity decay. In the developed sample, the protective layer and 3D structure provide void space to accommodate the big volumetric change during cycling.[33,34] As depicted in Figure 6b, morphology integrity of the coated spheres is preserved after cycling for 100 times. In contrast, the CZTS spheres of sample B have collapsed into enormous cracks.

Based on the above results, the excellent electrochemical properties of sample C can be understandably attributed to multiple factors:

(1) Various types of alloys and the additional Li^+ supplied by LiPON improve the capacity and conductivity;
(2) The artificial surface film prevents the CZTS film from directly contacting the electrolyte, reduces the dissolution of sulfides, and retards the growth of SEI layer; and
(3) The modified surface and 3D substrate strengthen the structural stabilization of CZTS clusters during cycling and therefore facilitate a remarkable cycle life.

4. CONCLUSIONS

For the first time, we have proposed a novel three-dimensional (3D) composite film LiPON/CZTS/Ni fabricated by magnetron sputtering and applied it to thin-film lithium-ion batteries (LIBs). Compared with the pure CZTS materials, the developed samples exhibit a greatly enhanced capacity and cycle life that result from the modified surface, the released volumetric expansion, and the reduced dissolution of sulfides. The significant results of the materials design and application from this study can contribute to the research of potential materials for advanced thin-film LIBs. To advance closer to practical applications, efforts in future work will focus on the incorporation of novel electrolyte and coatings with high conductivity.

■ ASSOCIATED CONTENT

Supporting Information

The Supporting Information is available free of charge on the ACS Publications website at DOI: 10.1021/acsami.5b04421.

Additional CV curves (PDF)

■ AUTHOR INFORMATION

Corresponding Author

*E-mail: hangguo@xmu.edu.cn.

Notes

The authors declare no competing financial interest.

■ ACKNOWLEDGMENTS

This work is financially supported by the Program for New Century Excellent Talents in University (No. 2007NCET-07-0723), Aeronautical Science Foundation of China (No. 2008ZH68002), and National Natural Science Foundation of China (No. 60936003).

■ REFERENCES

(1) Beidaghi, M.; Gogotsi, Y. Capacitive Energy Storage in Micro-Scale Devices: Recent Advances in Design and Fabrication of Micro-Supercapacitors. *Energy Environ. Sci.* **2014**, *7* (3), 867−884.
(2) Bates, J. B.; Dudney, N. J.; Neudecker, B.; Ueda, A.; Evans, C. D. Thin-Film Lithium and Lithium-Ion Batteries. *Solid State Ionics* **2000**, *135* (1−4), 33−45.
(3) Scrosati, B.; Garche, J. Lithium Batteries: Status, Prospects and Future. *J. Power Sources* **2010**, *195* (9), 2419−2430.
(4) Cabana, J.; Monconduit, L.; Larcher, D.; Palacin, M. R. Beyond Intercalation-Based Li-Ion Batteries: The State of the Art and Challenges of Electrode Materials Reacting through Conversion Reactions. *Adv. Mater.* **2010**, *22* (35), E170−E192.
(5) Yoshio, M.; Wang, H.; Fukuda, K.; Hara, Y.; Adachi, Y. Effect of Carbon Coating on Electrochemical Performance of Treated Natural Graphite as Lithium-Ion Battery Anode Material. *J. Electrochem. Soc.* **2000**, *147* (4), 1245−1250.
(6) Débart, A.; Dupont, L.; Patrice, R.; Tarascon, J. M. Reactivity of Transition Metal (Co, Ni, Cu) Sulphides Versus Lithium: The

DOI: 10.1021/acsami.5b04421
ACS Appl. Mater. Interfaces 2015, 7, 17311−17317

Intriguing Case of the Copper Sulphide. *Solid State Sci.* **2006**, *8* (6), 640−651.
(7) He, L.; Liao, X.-Z.; Yang, K.; He, Y.-S.; Wen, W.; Ma, Z.-F. Electrochemical Characteristics and Intercalation Mechanism of ZnS/C Composite as Anode Active Material for Lithium-Ion Batteries. *Electrochim. Acta* **2011**, *56* (3), 1213−1218.
(8) Li, Y.; Tu, J. P.; Wu, H. M.; Yuan, Y. F.; Shi, D. Q. Mechanochemical Synthesis and Electrochemical Properties of Nanosized SnS as an Anode Material for Lithium Ion Batteries. *Mater. Sci. Eng., B* **2006**, *128* (1−3), 75−79.
(9) Ritchie, A. G.; Bowles, P. G.; Scattergood, D. P. Lithium-Ion/Iron Sulphide Rechargeable Batteries. *J. Power Sources* **2004**, *136* (2), 276−280.
(10) Qu, B.; Zhang, M.; Lei, D.; Zeng, Y.; Chen, Y.; Chen, L.; Li, Q.; Wang, Y.; Wang, T. Facile Solvothermal Synthesis of Mesoporous Cu_2SnS_3 Spheres and Their Application in Lithium-Ion Batteries. *Nanoscale* **2011**, *3* (9), 3646−3651.
(11) Li, Y.; Tu, J. P.; Huang, X. H.; Wu, H. M.; Yuan, Y. F. Nanoscale SnS with and without Carbon-Coatings as an Anode Material for Lithium Ion Batteries. *Electrochim. Acta* **2006**, *52* (3), 1383−1389.
(12) Wang, L.; Kitamura, S.; Obata, K.; Tanase, S.; Sakai, T. Multilayered Sn−Zn−Cu Alloy Thin-Film as Negative Electrodes for Advanced Lithium-Ion Batteries. *J. Power Sources* **2005**, *141* (2), 286−292.
(13) Shinde, N. M.; Deshmukh, P. R.; Patil, S. V.; Lokhande, C. D. Aqueous Chemical Growth of Cu_2ZnSnS_4 (CZTS) Thin Films: Air Annealing and Photoelectrochemical Properties. *Mater. Res. Bull.* **2013**, *48* (5), 1760−1766.
(14) Du, Z. J.; Zhang, S. C.; Zhao, J. F.; Fang, Y. Investigation of Immiscible Sn-Zn Coatings with Two-Layer Microstructure as Anode Material for Li-Ion Battery. *J. Appl. Electrochem.* **2012**, *42* (7), 477−482.
(15) Bates, J. B.; Dudney, N. J.; Lubben, D. C.; Gruzalski, G. R.; Kwak, B. S.; Yu, X.; Zuhr, R. A. Thin-Film Rechargeable Lithium Batteries. *J. Power Sources* **1995**, *54* (1), 58−62.
(16) Dudney, N. J.; Neudecker, B. J. Solid State Thin-Film Lithium Battery Systems. *Curr. Opin. Solid State Mater. Sci.* **1999**, *4* (5), 479−482.
(17) Li, J. C.; Ma, C.; Chi, M. F.; Liang, C. D.; Dudney, N. J. Solid Electrolyte: The Key for High-Voltage Lithium Batteries. *Adv. Energy Mater.* **2015**, *5* (4), 1401408.
(18) Kang, B.; Ceder, G. Battery Materials for Ultrafast Charging and Discharging. *Nature* **2009**, *458* (7235), 190−193.
(19) Kim, Y.; Veith, G. M.; Nanda, J.; Unocic, R. R.; Chi, M. F.; Dudney, N. J. High Voltage Stability of $LiCoO_2$ Particles with a Nano-Scale Lipon Coating. *Electrochim. Acta* **2011**, *56* (19), 6573−6580.
(20) Chiu, K. F.; Lin, H. C.; Lin, K. M.; Chen, C. C. Stability Improvement of $LiMn_2O_4$ Thin-Film Cathodes under High Rate and Over-Discharge Cycling. *J. Electrochem. Soc.* **2006**, *153* (10), A1992−A1997.
(21) Li, J. C.; Baggetto, L.; Martha, S. K.; Veith, G. M.; Nanda, J.; Liang, C. D.; Dudney, N. J. An Artificial Solid Electrolyte Interphase Enables the Use of a $LiNi_{0.5}Mn_{1.5}O_4$ 5 V Cathode with Conventional Electrolytes. *Adv. Energy Mater.* **2013**, *3* (10), 1275−1278.
(22) Li, J. C.; Dudney, N. J.; Nanda, J.; Liang, C. Artificial Solid Electrolyte Interphase to Address the Electrochemical Degradation of Silicon Electrodes. *ACS Appl. Mater. Interfaces* **2014**, *6* (13), 10083−10088.
(23) Zhou, W.-H.; Zhou, Y.-L.; Feng, J.; Zhang, J.-W.; Wu, S.-X.; Guo, X.-C.; Cao, X. Solvothermal Synthesis of Flower-Like Cu_2ZnSnS_4 Nanostructures and Their Application as Anode Materials for Lithium-Ion Batteries. *Chem. Phys. Lett.* **2012**, *546*, 115−119.
(24) Li, J.; Shen, J.; Li, Z.; Li, X.; Sun, Z.; Hu, Z.; Huang, S. Wet Chemical Route to the Synthesis of Kesterite Cu_2ZnSnS_4 Nanocrystals and Their Applications in Lithium Ion Batteries. *Mater. Lett.* **2013**, *92*, 330−333.
(25) Yang, X.; Xu, J.; Xi, L.; Yao, Y.; Yang, Q.; Chung, C. Y.; Lee, C.-S. Microwave-Assisted Synthesis of Cu_2ZnSnS_4 Nanocrystals as a Novel Anode Material for Lithium Ion Battery. *J. Nanopart. Res.* **2012**, *14* (6), 931−936.
(26) Yin, X.; Tang, C.; Chen, M.; Adams, S.; Wang, H.; Gong, H. Hierarchical Porous Cu_2ZnSnS_4 Films for High-Capacity Reversible Lithium Storage Applications. *J. Mater. Chem. A* **2013**, *1* (27), 7927−7932.
(27) Patil, A.; Patil, V.; Wook Shin, D.; Choi, J.-W.; Paik, D.-S.; Yoon, S.-J. Issue and Challenges Facing Rechargeable Thin Film Lithium Batteries. *Mater. Res. Bull.* **2008**, *43* (8−9), 1913−1942.
(28) Guo, Q.; Ford, G. M.; Yang, W. C.; Walker, B. C.; Stach, E. A.; Hillhouse, H. W.; Agrawal, R. Fabrication of 7.2% Efficient CZTSSe Solar Cells Using Czts Nanocrystals. *J. Am. Chem. Soc.* **2010**, *132* (49), 17384−17386.
(29) Huang, G.; Chen, T.; Wang, Z.; Chang, K.; Chen, W. Synthesis and Electrochemical Performances of Cobalt Sulfides/Graphene Nanocomposite as Anode Material of Li-Ion Battery. *J. Power Sources* **2013**, *235*, 122−128.
(30) Bloom, I.; Trahey, L.; Abouimrane, A.; Belharouak, I.; Zhang, X. F.; Wu, Q. L.; Lu, W. Q.; Abraham, D. P.; Bettge, M.; Elam, J. W.; Meng, X. B.; Burrell, A. K.; Ban, C. M.; Tenent, R.; Nanda, J.; Dudney, N. Effect of Interface Modifications on Voltage Fade in $0.5Li_2MnO_3 \cdot 0.5LiNi_{0.375}Mn_{0.375}Co_{0.25}O_2$ Cathode Materials. *J. Power Sources* **2014**, *249*, 509−514.
(31) Winter, M.; Besenhard, J. O. Electrochemical Lithiation of Tin and Tin-Based Intermetallics and Composites. *Electrochim. Acta* **1999**, *45* (1−2), 31−50.
(32) Kim, Y.; Dudney, N. J.; Chi, M. F.; Martha, S. K.; Nanda, J.; Veith, G. M.; Liang, C. D. A Perspective on Coatings to Stabilize High-Voltage Cathodes: $LiMn_{1.5}Ni_{0.5}O_4$ with Sub-Nanometer Lipon Cycled with $LiPF_6$ Electrolyte. *J. Electrochem. Soc.* **2013**, *160* (5), A3113−A3125.
(33) Liu, N.; Lu, Z.; Zhao, J.; McDowell, M. T.; Lee, H. W.; Zhao, W.; Cui, Y. A Pomegranate-Inspired Nanoscale Design for Large-Volume-Change Lithium Battery Anodes. *Nat. Nanotechnol.* **2014**, *9* (3), 187−192.
(34) Seh, Z. W.; Li, W.; Cha, J. J.; Zheng, G.; Yang, Y.; McDowell, M. T.; Hsu, P.-C.; Cui, Y. Sulphur−TiO_2 Yolk−Shell Nanoarchitecture with Internal Void Space for Long-Cycle Lithium−Sulphur Batteries. *Nat. Commun.* **2013**, *4*, 1331−1336.

DOI: 10.1021/acsami.5b04421
ACS Appl. Mater. Interfaces 2015, 7, 17311−17317